

Surface Modification of Stretched TiO₂ Nanotubes for Solid-State Dye-Sensitized Solar Cells

Soon Hyung Kang, Jae-Yup Kim, Yukyeong Kim, Hyun Sik Kim, and Yung-Eun Sung*

School of Chemical and Biological Engineering and Interdisciplinary Program in Nano Science and Technology, Seoul National University, Seoul 151-742, Republic of Korea

Received: February 22, 2007; In Final Form: April 25, 2007

Straight-stranded anatase TiO₂ nanotubes were produced by anodic oxidation on a pure titanium substrate in an aqueous solution containing a 0.45 wt % NaF electrolyte (pH 4.3 fixed). The average length of the TiO₂ nanotubes was approximately 3 μm, which had an effect on the level of dye adsorption in the dye-sensitized solar cells. The anodic TiO₂ nanotubes were applied as a working electrode in a solid-state dye-sensitized solar cell. An approximately 1 nm ZnO shell was coated on the TiO₂ nanotube to improve the open-circuit voltage (V_{oc}) and conversion efficiency of the solar cell, and to retard any back reaction. Although the V_{oc} and short-circuit current (J_{sc}) of the cell were improved, there was a low fill factor as a result of the formation of a thick TiO₂ barrier layer in the anodic TiO₂/Ti substrate. A parameter on the degradation of fill factor (37%) is related to the formation of a thick TiO₂ barrier layer in the anodic TiO₂/Ti substrate interface. A hydrogen peroxide treatment was performed in an attempt to narrow the TiO₂ barrier layer. This treatment was found to influence not only fill factor (37–49%) but also the conversion efficiency (0.704–0.906%) of the cell by eliminating the remnant after anodic reaction and barrier narrowing through an etching effect. This result was confirmed by X-ray photoelectron spectroscopy (XPS) and photocurrent-voltage measurements. The longer electron lifetime on the ZnO coated TiO₂ film was measured by the open-circuit voltage decay. The improvement in the electron lifetime from the thin ZnO coating affects the number of electrons collected on the Ti substrate and the retardation of charge recombination. Therefore, the ZnO coating on the TiO₂ nanotube film improves the efficiency of dye-sensitized TiO₂ solar cells from the extended V_{oc} from ZnO coating confirmed by the Mott–Schottky plots and the increased J_{sc} through the inhibition of charge recombination confirmed by IPCE measurements.

1. Introduction

Self-organized porous metal oxides (Al₂O₃, TiO₂, ZrO₂, etc.) with a nanotubular structure have attracted significant interest in recent years. In particular, the favorable physical, optical, and electrical properties of TiO₂ make it possible to apply anodically formed TiO₂ nanotubes to various fields requiring an interconnected and large internal surface area, such as photovoltaic devices,^{1–3} electrochromic windows,⁴ photocatalysts,⁵ and Li ion batteries.^{6–7} Although considerable research has been concentrated on the development of nanotubular TiO₂ layers, there is no simple synthesis route to obtain a uniformly stretched nanotubular structure with the exception of an electrochemical anodization process.^{8–9} This fabrication technology is quite useful due to its low cost, large area fabrication, good mechanical adhesion, and electrical conductivity due to the nanotubes being directly connected to the substrate.¹⁰ Furthermore, straight-stranded TiO₂ nanotubes suppress the loss of electron transport originating from many grain boundaries in a film composed of interconnected titania particles, which leads to an improvement in efficiency due to the increased surface area on the interior and exterior walls of the nanotubes in dye-sensitized solar cells.

An efficiency > 15% is required to accelerate the practical use of dye-sensitized solar cells and make them competitive with Si-based solar cells. Up to now, the efficiency of dye-

sensitized solar cell has reached as much as 11%.¹¹ One of the factors limiting the performance of dye-sensitized solar cells is related to electron transport in nanoparticle TiO₂ films.¹² The 10 μm-thick nanostructured TiO₂ film is now being used as the electron transporting layer consists typically of interconnected nanometer-sized TiO₂ particles (in the size range of 5–50 nm) with a high internal surface area. The large surface area increases with increasing thickness of the nanoporous TiO₂ film, while the loss of electron transport through the randomly distributed 3-D network also increases due to the presence of more grain boundaries and limited diffusion length.¹³ A vertically oriented anodic TiO₂ film might be appropriate for enhancing electron transport in TiO₂ films.¹⁴

However, Frank's group¹⁵ examined the characteristics of electron transport in TiO₂ nanotube and nanoparticle-based dye-sensitized solar cells. Surprisingly, the transport times for both samples were comparable, reflecting the similar average crystallite size. This may also be the result of the similar nanostructured morphology, except for the dimensional difference in composed TiO₂ materials. In particular, the grown TiO₂ nanotube showed the typical wall thickness (15–20 nm) intertube spacing (8–10 nm) and pore diameter (30 nm), and a similar morphology with the exception of directly stretched configuration. Electrons in the nanotube also encounter many grain boundaries, defects, and trap sites, becoming a factor that retards the electron transport time. This means that there are limitations in length in the TiO₂ nanotube for application to dye-sensitized solar cells, which is comparable to nanoparticle-based dye-sensitized solar cells.

* Corresponding author. Tel: +82-2-880-1889. Fax: +82-2-888-1604. E-mail: ysung@snu.ac.kr.

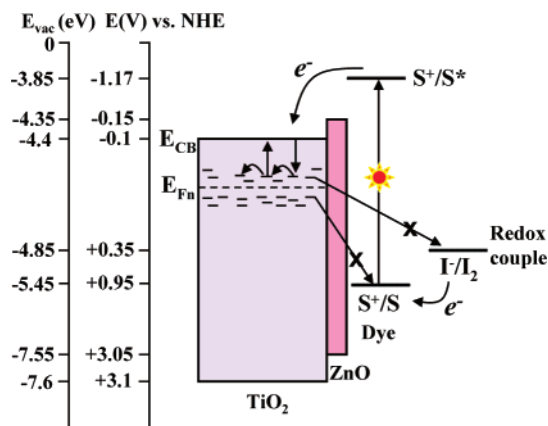


Figure 1. Interfacial charge-transfer process at the ZnO coated TiO₂/dye/electrolyte of DSSC. Trapping/detrapping events of photoinjected electrons between the conduction band and trap sites of TiO₂ were described in the region of E_{Fn}.

Furthermore, charge recombination at the interface of the electrode/electrolyte may lead to the use of more sophisticated device architectures for improved efficiency and long-term stability. One of interesting methods for suppressing the charge recombination is to coat the TiO₂ film with wide band gap metal oxides (ZnO, Al₂O₃, SnO₂, Nb₂O₅, MgO, etc.).^{16–18} Because the main reason for using nanodimensional TiO₂ nanoparticles is to enlarge the dye uptake, the surface states on the TiO₂ nanoparticles, which provide shorter pathway to easily recombine with the cations of the redox electrolyte due to the close distance in the energetic band gap, may be not ignored, as shown in Figure 1. Since the photoinjected electrons flow not only through the conduction band of TiO₂, but also through the trap sites (e.g., surface states) distributed below the conduction band, thousands of trapping/detrapping events of photoinjected electrons occur before the electrons reach the transparent conducting oxide (electron collector). The electrons in the trap sites easily recombined with the redox electrolyte before the detrapping event, because the detrapping rate is slower than the trapping rate.¹⁹ The formation of an inherent energy barrier by coating with wide band gap materials as a shell at the electrode/electrolyte interface is essential for increasing the physical separation of the injected electrons from the cations of the redox electrolyte, thereby decreasing the rate of charge recombination.

In this study, an approximately 1 nm-thick ZnO shell, as a barrier layer, was coated on the anodic TiO₂ nanotubes using electrochemical deposition, contributing to the suppression of charge recombination and the increase in the V_{oc} through a negative shift (toward vacuum level) of V_{CB} in the TiO₂. The negative shift (toward vacuum level) of V_{CB} in the TiO₂ was verified by the Mott–Schottky plots. In particular, the thin ZnO layer also reduced the number of Ti³⁺ in the surface region. Moreover, the low fill factor was overcome by a hydrogen peroxide (10 mM) treatment, which reduced the TiO₂ barrier thickness and etching effect of the TiO₂ surface.

2. Experimental Section

2.1. Preparation of Anodic TiO₂ Film. A 0.5 mm-thick titanium sheet (99.9% purity, Nikko Metal, Japan) was cleaned by sonicating it successively in acetone, ethanol, and deionized (DI) water, for 10 min each, followed by drying in an air stream. A 1.5 cm × 2 cm specimen of the Ti sheet was cut and a copper wire was attached to the upper front side using a conducting epoxy adhesive. After drying, all areas except for the actual 1 cm² exposure area on the front side were pasted with a

nonconducting epoxy adhesive on both sides and dried in an oven. Constant voltage anodization was then performed using a two-electrode configuration with a working electrode made from a Ti sheet and a counter electrode made from Pt wire. The reason for using the three-electrode configuration system is to minimize the ohmic drop (IR_s), which is as a type of voltage drop in the interface of the working and counter electrodes that influences the electrochemical reaction.²⁰ The representative causes are due to the resistance of electrolyte and the distance between the working and counter electrodes. However, the anodic reaction is positioned to overcome the problems of the two-electrode configuration because the electrolyte used is sufficiently conductive in the 0.5 M Na₂SO₄ supporting electrolyte, and the applied voltage as a driving force for ions motion is sufficiently large to minimize the resistance of the electrolyte.

All the experiments were carried out at approximately 23 °C at an applied voltage of 20 V for 18 h. The composition of the electrolyte was 0.5 M Na₂SO₄, 0.5 M H₃PO₄, 0.2 M sodium citrate and 0.45 wt % NaF solution under slow magnetic agitation (150 rpm). The pH was adjusted to approximately 4.3 (±0.05) by NaOH. The anodized samples were washed and sonicated in DI water for 5 min to remove the remnants of the anodic reaction and annealed at 450 °C (heating/cooling rate of 1.5 °C/min) for 4 h under air ambient.

2.2. Electrode Assembly. The annealed nanotubular TiO₂ film was treated with 10 mM hydrogen peroxide (H₂O₂) (Junsei, Japan, diluted from 30 wt %) for 10 min and washed with DI water, followed by drying in an air stream. All the chemicals were of analytical grade. The photoelectrodes were immersed in an acetonitrile solution containing 5×10^{-4} M *cis*-bis-(isothiocyanato)bis(2,2'-bipyridyl-4,4'-dicarboxylato)-ruthenium-(II)bis-tetrabutylammonium (Ru 535-bisTBA, Solaronix) for at least 12 h at 60 °C in an oven. The electrode was then rinsed with acetonitrile and dried under an air stream.

The nanofiller particle-inserted (nanosized SiO₂ or TiO₂ particles) polymer electrolyte was actively investigated in an attempt to improve the ionic conductivity and cause a high interfacial contact. The nanofiller particles prevented recrystallization and decreased the level of crystallinity. The solid-state polymer electrolyte for the silica nanoparticles was prepared consisting of low molecular weight poly(ethylene oxide dimethyl ether) (PEODME, $M_w = 500$ g/mol, $R_g = 1.4$ nm), fumed silica nanoparticles (20 nm, Degussa), imidazolium iodide, iodine, and acetonitrile as a volatile solvent.²¹ This mixture was stirred for more than 12 h and the solvent was evaporated at a temperature of 60 °C in an oven. The Pt coated counter electrodes were prepared by spreading a drop of 5 mM H₂PtCl₆ in 2-propanol onto fluorine-doped SnO₂ (FTO) films (Pilkington TEC Glass, sheet resistance 8 Ω/square, transmittance 77% in the visible range) and heating it to 400 °C for 15 min under air ambient. Only one-side of the dye-adsorbed TiO₂ electrodes (active area 0.25 cm²) was pressed using a thermal adhesive film (Serlyn, thickness: 60 μm). It should be noted that all areas containing the space where the electrolyte was connected directly to the Ti substrate, except for the active area, must be covered by a Serlyn film to prevent a decrease in V_{oc} . Finally, the polymer electrolyte solution was cast on the dye adsorbed TiO₂ electrode that had been covered by the Pt coated counter electrode in the aid of clamps.

2.3. Photoelectrochemical Measurements. The photovoltaic characteristics were analyzed using a 500 W xenon lamp (XIL model 05A50KS source units laid on AM 1.5 filter) with a light intensity of 1 sun (100 mW/cm²), which was adjusted using a

NREL fabricated Si reference solar cell. A 50 μm thick polyester film was coated on the cell as a UV cutoff filter (up to 400 nm).

The incident photon to current conversion efficiency (IPCE) were collected under short circuit conditions with a tungsten lamp source and a 10 nm bandwidth monochromator, which resulted in an illumination intensity of approximately 1 mW/cm².

2.4. Electrochemical Measurements. The electrochemical measurement was performed using a three-electrode system at 25 °C. The anodic TiO₂ electrode (geometric surface area 1 cm²), a saturated Ag/AgCl electrode and a platinum wire were used as the working, reference, and counter electrode, respectively. In this case, the three-electrode configuration was used to minimize the ohmic drop because of the limited range of the scanned voltage. The anodic TiO₂ film was then heated in an oven at 80 °C for 10 min to remove any adsorbed moisture and organics before scanning the potential. Nitrogen bubbling was essential for removing any oxygen present in the electrolyte that would influence the potential of the redox reaction by acting as an oxidizing agent.²² In order to detect the interfacial electron transfer related reaction in the anodic TiO₂ film/electrolyte, cyclic voltammetry (CV) was performed at a potential ranging from +0.8 to -0.8 V versus Ag/AgCl in a 0.1 M NaOH solution (pH 13) at a scan rate of 50 mV/s. Electrochemical deposition carried out in solution containing 0.15 M LiNO₃, 0.005 M Zn(NO₃)₂ hydrate, and 0.05 M ZnCl₂ in propylene carbonate was applied to coat a thin ZnO material on the TiO₂ surface. After nitrogen bubbling to remove the water and moisture in the organic based solvent, one cycle between 0 and -1.4 V versus a saturated Ag/AgCl reference electrode was scanned at a scan rate of 50 mV/s according to the procedure reported elsewhere.²³ After scanning, the sample was washed thoroughly in an ethanol solution and annealed at 450 °C (heating/cooling rate 1.5 °C/min) for 30 min under air ambient to promote a chemical reaction.

In order to determine the flatband potential (V_{FB}) of the semiconducting TiO₂ film, Mott-Schottky plots were obtained in a three-electrode cell using bare TiO₂ and ZnO coated TiO₂ photoanodes, a platinum wire, and an saturated Ag/AgCl as the working, counter and reference electrodes, respectively. To make the active cell, all area except for the active area (1 cm²), was cast using a nonconducting epoxy in both sides. The electrolyte containing 0.2 M LiClO₄ in acetonitrile (AN) (pH 6.2) was used and nitrogen bubbling was carried out before taking the measurements.²⁴ The electrochemical impedance spectra were obtained applying a sinusoidal perturbation of ± 10 mV at a frequency of 1 kHz and a cell voltage of 0 V using a Zahner impedance analyzer controlled by a PC.

The electron lifetimes in the bare and ZnO coated anodic TiO₂ films were determined by measuring the open-circuit voltage decay (OCVD) as soon as the stationary illumination had been interrupted, and the change in $V_{\text{oc}}(t)$ was recorded. The electron lifetime was calculated using the following eq 1:²⁵

$$\tau = -\frac{k_{\text{B}}T}{e} \left(\frac{dV_{\text{oc}}}{dt} \right)^{-1} \quad (1)$$

where $k_{\text{B}}T$ is thermal energy, e is the electronic charge, and dV_{oc}/dt is the derivative of the open-circuit voltage transient. The decays were recorded during relaxation from an illuminated quasi-equilibrium state to a dark equilibrium. The transient of V_{oc} induced by the large variation in the photophysical magnitudes provides information on the properties of the recombination process, which coincides with the results mea-

sured using the small signal frequency domain technique (incident-modulated photovoltage spectroscopy, IMVS).²⁶ Accordingly, the process for interfacial charge recombination along the all ranges of the scanned potential was interpreted using this technique.

2.5. Characterization. X-ray photoemission spectroscopy (XPS) (PHI 5200 mode) was performed to examine the chemical bonding states at the anodic TiO₂/ZnO interface and the passivation effect of oxygen vacancies induced by the Ti³⁺ state after the hydrogen peroxide treatment using an Al K_{α} X-ray source in a chamber base pressure of $\sim 10^{-10}$ Torr. High-resolution transmission electron microscopy (HR-TEM) (JEOL JEM-2010) at 200 keV was used to examine the morphology of the anodic TiO₂ nanotubes. The surface compositions of the samples were analyzed using energy dispersive spectroscopy (EDS). The thickness and morphology of the anodic TiO₂ nanotubes were confirmed using a JSM-6330F field emission scanning electron microscope (FE-SEM, JEOL Inc.) operating at 10 kV and 20 mA. The crystalline phase and structure was confirmed using high power X-ray diffraction (Rigaku D/MAX 2500 V diffractor) with Cu K_{α} radiation operating at 40 kV and 100 mA. Atomic force microscopy (AFM) using a Nanoscope IIIa (Dimension 3100) with an etched silicon cantilever in the tapping mode was used to examine the surface roughness of the anodically grown TiO₂ film. The scans were extended over $5 \times 5 \mu\text{m}^2$ areas. The absorbance spectra were obtained using a Shimadzu model 3100 UV-vis spectrophotometer at a wavelength ranging from 350 to 800 nm at room temperature.

3. Results and Discussion

3.1. Morphological Characterization. Figure 2 shows the FE-SEM images of the self-ordered porous TiO₂ with a length of approximately 3 μm . The average diameter of the nanotubes was 100 nm (± 20 nm) with a wall thickness of 20 nm (± 5 nm). The image shows a morphology consisting of a wide range of TiO₂ nanotube lengths. This surface roughness caused by the difference in nanotube length increased with increasing pH in the electrolyte, shown in Figure S1. It was reported that the growth of the rough TiO₂ nanotubes were processed repetitively. Initially, pore formation was initiated at the breakdown sites, followed by the growth of pores with various growth rates. The porous TiO₂ nanotubes are grown as the samples were continuously anodized. It is possible that small pores are formed in the tubes during the repetitive processes, i.e., the formation of a barrier oxide layer, the breakdown of oxides, passivation of the breakdown sites, breakdown of the passivated oxide layer, and repassivation, etc.²⁷ The nanotubes containing small pores become partially swollen on the bottom of the pores due to the sudden increase in the anodic current. These swollen pores also continued to grow under the equilibrium state between the chemical oxidation and chemical dissolution process.

At a specific point (e.g., where the anodic current suddenly increased), the swollen pores separated to produce two TiO₂ nanotubes, one long and one short. As a result, the separated short TiO₂ nanotubes induced the formation of an irregular surface morphology. The pores were interconnected, while the dominantly stretched TiO₂ nanotubes were bent in the downward direction, which suggests that the nanotubes continued to grow competitively under a constant stress.²⁸ The TiO₂ ridges that formed at constant intervals links the independently separated nanotubes, which might be essential for electron transport in a dye-sensitized solar cell. In addition, an open pore mouth and closed pore bottom were observed, which is similar to the previously reported results.²⁹ A thin compact TiO₂ layer between

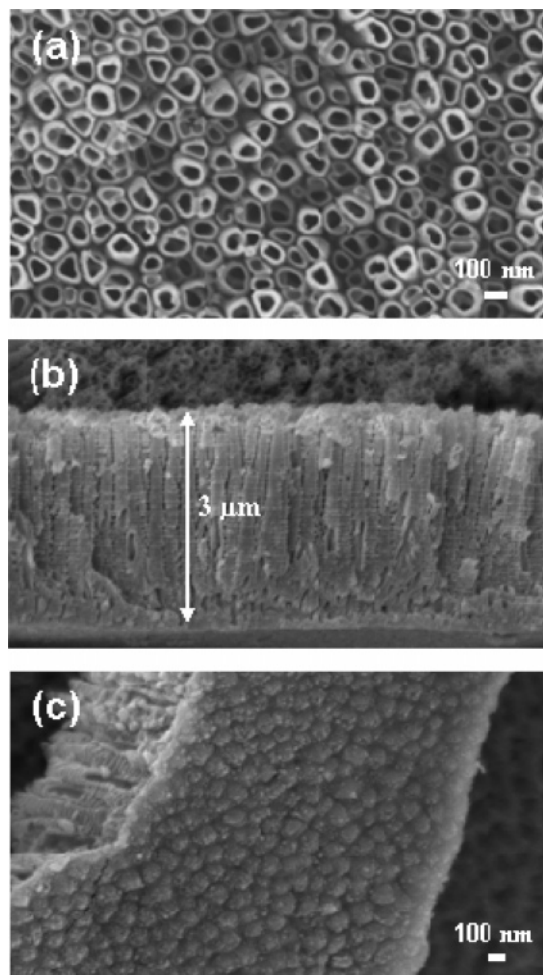


Figure 2. FE-SEM images showing the formation of highly ordered TiO₂ nanotubes based on the aqueous electrolyte (0.45 wt % NaF + 0.5 M H₃PO₄ + 0.5 M Na₂SO₄ + 0.2 M sodium citrate) with the pH adjusted to 4.3 (± 0.05) by the NaOH reagent; (a) top-view, (b) cross-sectional view, and (c) bottom view of the TiO₂ nanotubes.

the TiO₂ nanotube and the Ti substrate viewed in closed bottom was formed, and became a pathway for the photojected electrons to tunnel to the Ti substrate. From the bottom view, all the nanotubes are connected, terminating the anodic reaction in the same configuration of the nanotube.

HR-TEM analysis was carried out to observe the detailed growth process. Figure 3 shows the morphology of nanotubular TiO₂ and thin ZnO covering on the titanium oxide surface. An approximately 1 nm-thick ZnO shell (0.4 at %) was coated on the TiO₂ nanotubes, as confirmed by electron diffraction spectroscopy (EDS). Selective area electron diffraction (SAED) analysis demonstrated that the annealed TiO₂ nanotubes were anatase.

3.2. Crystal Structure of Anodic TiO₂ Film. As shown in Figure 4, the XRD pattern of the as-anodized nanotubes showed no crystalline phases; only the peaks associated with the Ti substrate. This suggests that an amorphous phase had formed. The amorphous phase transformed to anatase phase after the long-term thermal treatment in air ambient, as shown by the (101), (004), (200), and (105)(211) planes. The annealing process also provides the high crystalline properties of the anodic titania film, while the intensity of the peaks related to the Ti substrate was reduced. The average crystallite size (35.2 nm) was calculated using the Scherrer equation³⁰ ($L = 0.9 \cdot \lambda_{\text{K}\alpha} / B(2\theta) \cdot \cos\theta_{\text{max}}$, where L is the average crystallite size, $\lambda_{\text{K}\alpha}$ is the wavelength (1.54056) of the CuK α line, $B(2\theta)$ is the full width

at half maximum (fwhm) in radians, and θ is the Bragg angle) from the anatase (101) peak at $2\theta = 25.3^\circ$. This size corresponds to about two times, compared with that of conventional TiO₂ nanoparticles (15–20 nm).

3.3. XPS. The chemical changes caused by the thin ZnO coating on the surface region of anodic TiO₂ nanotube was examined by XPS, (Figure 5) after sputtering (5–6 Å) to remove all surface contamination. In the lightly sputtered samples, there was no change in the peak width and shift in the peak position, compared with the bare samples. Figure 5a shows the spectra of the bare and ZnO coated TiO₂ film over the wide scan range. The composition of both samples was composed of mainly Ti (458.5 eV of Ti 2p_{3/2}), O (531.6 eV of O 1s) and F (684.9 eV of F 1s), C (284.3 eV of C 1s) at extremely small surface concentrations. Zn (1021.7 eV of Zn 2p_{3/2}) was observed on the ZnO coated TiO₂ nanotube, which provides evidence for the formation of a ZnO layer on the anodic TiO₂ nanotube.

Figure 5b shows the Zn 2p_{3/2} core level peak of the bare and ZnO coated TiO₂ samples. The Zn 2p_{3/2} peak at approximately 1021.7 eV was assigned to the Zn–O bond as the main peak in the XPS spectra of ZnO.³¹ This demonstrates that the electrochemical deposition of Zn material in the nanodimensional scale encourages ZnO covering on the TiO₂ surface after thermal treatment in air ambient. The narrow range scans of the Ti 2p core level peaks were also performed on both samples, as shown in Figure 5c. The Ti 2p core peak (458.5 eV of Ti 2p_{3/2}) of the bare sample conforms to that of the published data.²⁹ On the other hand, the Ti 2p core level of ZnO coated sample shifted to a higher binding energy side (approximately 0.3 eV) is from the high electron affinity of ZnO.³² Moreover, the slightly asymmetric peak with a weak shoulder on the low binding energy side (approximately 457 eV) of the main peak indicated the partial presence of Ti³⁺.³³ The presence of Ti³⁺ is attributed to the increase in the concentration of oxygen vacancies. The Ti³⁺ centers with a strong chemical activity allow the migration of the excessive electrons to the oxygen of the carboxylate group in the dye molecules, forming a chemically strong coordination bonding and offering additional space for the adsorption of dye molecules, which might increase the amount of dye adsorption. This result was confirmed in the following section. In addition, the minor formation of Ti³⁺ suggests the formation of two different oxidation states of oxygen (data not shown), which influence on charge transfer and the adsorption of dye molecules.

3.4. Solar Cell Characterization. Figure 6 shows the I – V characteristics of the solid-state dye-sensitized solar cells under illumination and in the dark state. The bare anodic TiO₂ electrode showed a V_{oc} of -0.64 V, a J_{sc} of 2.38 mA/cm², a fill factor of 38%, and an efficiency of 0.578%. On the other hand, the ZnO coated TiO₂ electrode showed a V_{oc} of -0.71 V, a J_{sc} of 2.68 mA/cm², a fill factor of 37%, and an efficiency of 0.704%. The thin ZnO coating enhances the conversion efficiency of the solid-state dye-sensitized solar cell. In particular, the increase in V_{oc} (V) might be due to the movement of the TiO₂ conduction band to negative direction, which is related to the formation of a barrier layer at the TiO₂ surface.³⁴ Moreover, the thin ZnO barrier layer suppresses charge recombination between the photojected electrons of TiO₂ and the triiodide ions of the redox electrolyte, resulting in an improvement in the V_{oc} of the cell.

According to a previous study,³⁵ the improvement in photocurrent was attributed to the decrease in electron loss in the electron transfer in the interface of the anodic TiO₂ electrode/electrolyte. Although the improvement in photocurrent does not correspond to any significant increase in the amount of dye

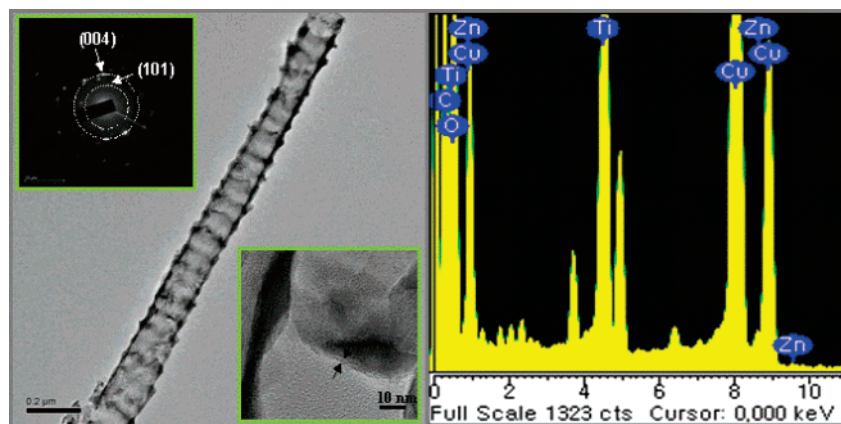


Figure 3. HR-TEM images of the anodic TiO₂ nanotubes, together with an enlarged view of the ZnO coated surface in the right down inset. Left top inset shows SAED pattern of an annealed TiO₂ film. The left side indicates quantitative surface composition of ZnO coated TiO₂ film by EDS.

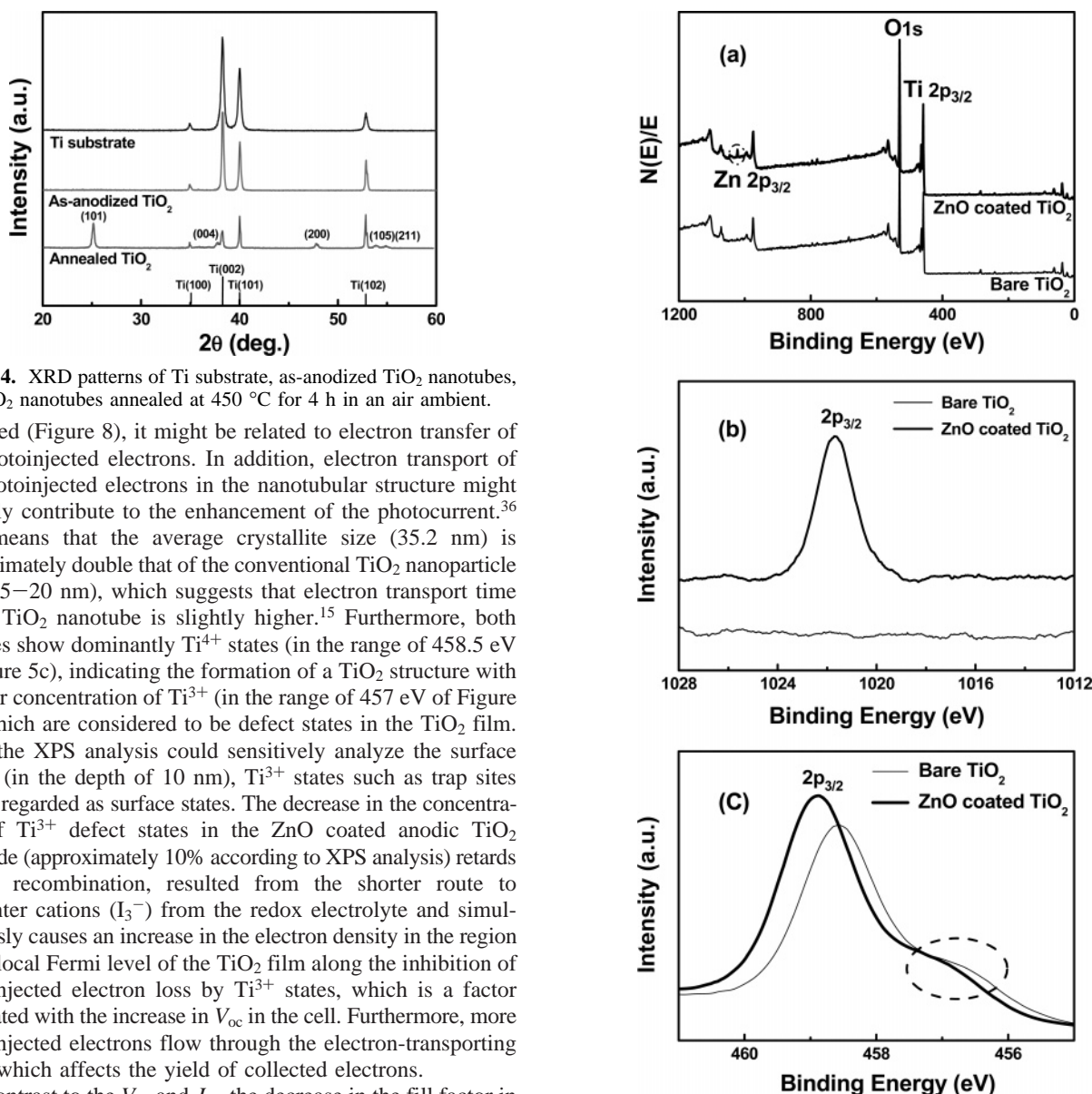


Figure 4. XRD patterns of Ti substrate, as-anodized TiO₂ nanotubes, and TiO₂ nanotubes annealed at 450 °C for 4 h in an air ambient.

adsorbed (Figure 8), it might be related to electron transfer of the photoinjected electrons. In addition, electron transport of the photoinjected electrons in the nanotubular structure might partially contribute to the enhancement of the photocurrent.³⁶ This means that the average crystallite size (35.2 nm) is approximately double that of the conventional TiO₂ nanoparticle size (15–20 nm), which suggests that electron transport time in the TiO₂ nanotube is slightly higher.¹⁵ Furthermore, both samples show dominantly Ti⁴⁺ states (in the range of 458.5 eV of Figure 5c), indicating the formation of a TiO₂ structure with a minor concentration of Ti³⁺ (in the range of 457 eV of Figure 5c), which are considered to be defect states in the TiO₂ film. Since the XPS analysis could sensitively analyze the surface region (in the depth of 10 nm), Ti³⁺ states such as trap sites can be regarded as surface states. The decrease in the concentration of Ti³⁺ defect states in the ZnO coated anodic TiO₂ electrode (approximately 10% according to XPS analysis) retards charge recombination, resulted from the shorter route to encounter cations (I₃⁻) from the redox electrolyte and simultaneously causes an increase in the electron density in the region of the local Fermi level of the TiO₂ film along the inhibition of photoinjected electron loss by Ti³⁺ states, which is a factor associated with the increase in V_{oc} in the cell. Furthermore, more photoinjected electrons flow through the electron-transporting layer, which affects the yield of collected electrons.

In contrast to the V_{oc} and J_{sc} , the decrease in the fill factor in both cells can be explained by a thickening of the barrier oxide layer in the TiO₂/Ti interface³⁷ and the resistance of the polymer electrolyte.³⁸ It was reported that a thin ZnO coating on an nanoporous TiO₂ film improved the fill factor in the dye-sensitized solar cell, thereby retarding charge recombination.³⁹ However, an improvement in the fill factor in the anodic TiO₂

Figure 5. XPS of bare TiO₂ and ZnO coated nanotubes in (a) the wide scan range and (b) the Zn 2p core level peak and (c) the Ti 2p core level peak of both samples after sputtering for 10 s.

film modified by ZnO coating was not expected due to the second-step thermal treatment. This might increase the TiO₂ barrier layer thickness in the Ti/TiO₂ interface, which would

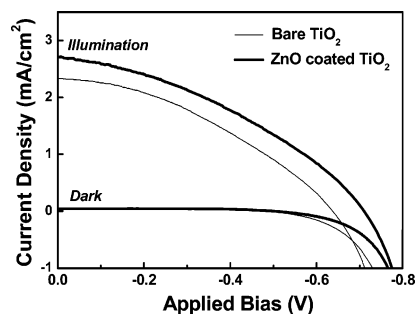


Figure 6. Photocurrent–voltage ($I-V$) characteristics in the illumination and dark states. (Light intensity, $100 \text{ mW}/\text{cm}^2$; AM, 1.5 filter; illumination area, 0.25 cm^2 .)

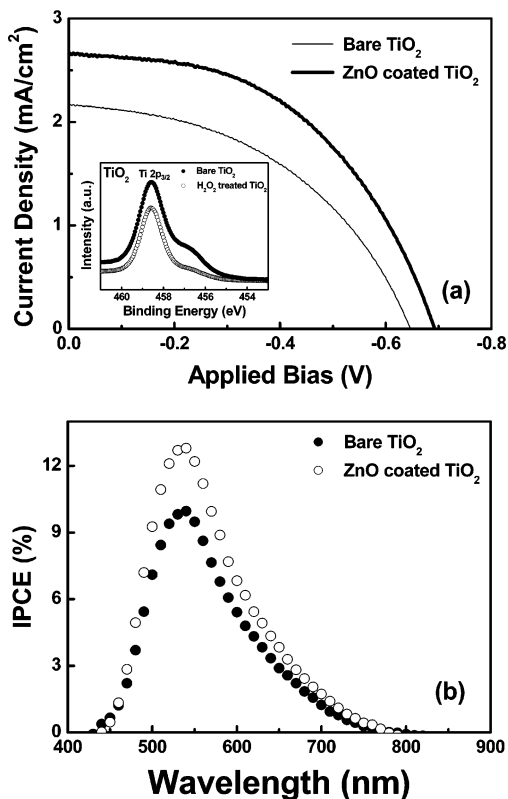


Figure 7. (a) Photocurrent–voltage ($I-V$) characteristics of $10 \text{ mM H}_2\text{O}_2$ treated TiO₂ and ZnO coated TiO₂ nanotubes in the light intensity of $100 \text{ mW}/\text{cm}^2$ with AM 1.5 filter (Active area: 0.25 cm^2). The inset of panel a indicates the XPS data before and after the H_2O_2 treatment of the nanotubular TiO₂ film. (b) IPCE spectra of $10 \text{ mM H}_2\text{O}_2$ treated TiO₂ and ZnO coated TiO₂ nanotubes (active area: 0.6 cm^2).

impede electron tunneling to the electron collecting layer (Ti substrate).^{40–42} It should be noted that the slow heating and cooling rate in the process of high-temperature thermal treatment is a key factor. A thicker barrier layer might be formed if such conditions are not present. Besides, the long-term annealed samples experienced shrinkage on the bottom layer of the tubes due to fusion of the adjacent nanotubes. This event continues to rise up to the pore mouth during the long-term thermal treatment. Hence, there is a decrease in the active area for the adsorption of dye molecules, which blocks electrolyte penetration. The low photocurrent of the cell composed of an anodically formed TiO₂ working electrode, compared with a nanoporous TiO₂ film suggests that the total area, containing the interior and exterior walls of the nanotubes cannot contribute to the active area for dye adsorption. This leads to an obstruction of the favorable penetration of polymer electrolyte to the space between the adjacent pores and Ti metal as an electron collector.

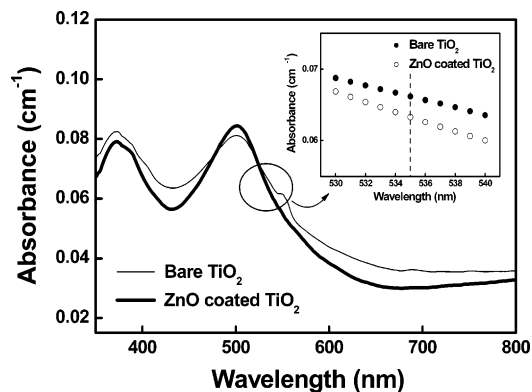


Figure 8. UV–vis spectra of desorbed dye molecules in 1 M NaOH solution with $10 \text{ mM H}_2\text{O}_2$ treated bare TiO₂ and ZnO coated TiO₂ samples. Inset shows magnified view in the range of 535 nm wavelength.

These points can explain the reasons for the low efficiency of the solid-state dye cell, compared with the nanoporous TiO₂ film at the same thickness. The low conductivity of the composite polymer electrolyte ($\sim 10^{-4} \text{ S}\cdot\text{cm}^{-1}$) and the latent solvent not being evaporated can be a reason for the low fill factor.^{43–44} The approximately 20% increase in the fill factor in liquid electrolyte-based cell was confirmed to induce to a 22% increase in efficiency in the dye solar cell, which corresponded to no change in the photovoltage and photocurrent.

Back-side illumination through the solid-state electrolyte side is needed to measure the conversion efficiency of the cell, which results from the nontransmittance of light through the Ti substrate. Generally, a 20% increase in the efficiency of a DSSC was expected with illumination occurring through transparent front side illumination.⁴⁵ The degraded efficiency on the back-side illumination can be explained by the high recombination loss during the transport of photoinjected electrons in the inner part of the nanostructured film. This shows that the photons at a longer wavelength have a weak influence on the photocurrent due to the decreased absorption through the many scattering events and the low extinction coefficient of the dye. In contrast, the photons at wavelengths ranging from 500 to 600 nm with a high absorption coefficient can travel a long distance within the film before reaching the current collector. For a film composed of nanoporous TiO₂ particles, a large proportion of the photoinjected electrons are lost due to charge recombination during electron transport, similarly, the electrons in the nanotubes experience similar electron transport events between the grain boundaries originating from the polycrystalline TiO₂ film, even though electrons are inclined to travel directly along the wall of the straight-lined nanotube instead of the configuration of a randomly distributed 3-D sphere.

Therefore, in order to compensate for the amount of charge recombination under back-side illumination, a gain of more light by adsorbing more dye molecules or an increase in the number of favorable surface states of the anodic TiO₂ nanotubes for the adsorption of dye molecules are important. The absorption of the electrolyte and reflection losses of the Pt counter electrode are responsible for only 5% of the degradation of the efficiency. The possible point of TiO₂ nanotubes in the application of a DSSC is the reduced loss of electron transport induced by the grain boundaries, and structural disorder between nanoparticles.⁴⁶ It is expected that this may compensate for the decreased efficiency through back-side illumination. On the other hand, a high efficiency of approximate 2.9% has been reported using only a 500 nm thick-TiO₂ nanotube coating in the conducting front side.⁴⁷ Hence, optimization of each part in the cell is

TABLE 1: The Summarization of I – V Properties in the Sample before and after Hydrogen Peroxide Treatment Measured under Solar Illuminated State^a

		V_{oc} (V)	J_{sc} (mA/cm ²)	fill factor (%)	efficiency (%)
bare	no treated	−0.64	2.38	38	0.578
ZnO coating		0.71	2.68	37	0.704
bare	10 mM H ₂ O ₂ treated	−0.646	2.17	45.7	0.640
ZnO coating		−0.693	2.67	49	0.906

^a The intensity of 100 mW/cm² with AM 1.5 G and active area of 0.25 cm² is used.

essential. In particular, the role of the TiO₂ blocking layer in the TiO₂/Ti interface and the formation of Ti³⁺ states to a DSSC need to be recognized.

3.5. Effects of the H₂O₂ Treatment. An acidic H₂O₂ treatment was carried out to determine the roles of the thick TiO₂ barrier in the TiO₂/Ti interface. After the first thermal treatment, the sample was dipped in a 10 mM H₂O₂ solution for 10 min. After washing with deionized water and drying in an oven at 60 °C for 30 min to remove the adsorbed moisture, the sample was dipped into an acetonitrile-based dye solution. Figure 7a shows the I – V curve of the samples of TiO₂ and ZnO coated TiO₂ treated with the acidic H₂O₂ solution. Table 1 shows the results concerning the properties of the solid-state dye-sensitized solar cell. The H₂O₂ treatment influences the factors affecting the efficiency, particularly the improved fill factor (about 30%), which is linked directly to an increase in conversion efficiency. This may result from the etching effect of the acidic H₂O₂ treatment on the TiO₂ film, causing a decrease in the thickness of the barrier layer, complete separation of each nanotube in the bottom region of the pore, and the elimination of the remnants anodic reaction (F and S elements), as confirmed by XPS (not shown here).

In the case of the H₂O₂ treated uncoated sample, the slightly reduced photocurrent may be due to the passivation of Ti³⁺ state which supplies the additional sites for dye adsorption through the formation of oxygen vacancies in the TiO₂ lattice. The inset in Figure 7a shows the XPS result before and after the 10 mM H₂O₂ treatment. The sample after the H₂O₂ treatment shows a well-passivated TiO₂ surface state with a binding energy of 457.7 eV. It also was reported that the carboxylate group of the dye molecules coordinates the surface TiO₂ atoms, resulting in the overlap of the ligand orbitals with the titanium atom.⁴⁸ The partially passivation of Ti³⁺ states on the TiO₂ surface was then induced and the remaining defect sites on the surface may be eliminated during the process of dye adsorption. Moreover, the oxidizing agent, H₂O₂, supplies oxygen with anionic properties to fill the vacant oxygen spaces, resulting in a negative shift in the band edge and a decrease in the photocurrent induced by the removal of the adsorption sites of the dye molecules. In contrast, the photovoltage of the cell was barely changed in the H₂O₂ treated uncoated sample.

This is from the compensation effect between the negative shift in the band edge from the filling of oxygen molecules and the adsorption of dissolved protons (H⁺) in the acidic hydrogen peroxide. Similar to the adsorption of Li⁺ ions as an adsorptive hard cation,⁴⁹ enough H⁺ ions influence the local photovoltage of the cell. The ZnO coated sample after the hydrogen peroxide treatment after an additional annealing process shows a minor decrease in the photovoltage. Overall, the acidic H₂O₂ treatment improves the fill factor, linking to the increase in conversion efficiency (about 30%) in the solid-state dye-sensitized solar cells, not corresponding to the significant decrease in the photovoltage and photocurrent.

Figure 7b shows the incident photon to current conversion efficiency (IPCE) as a function of the illumination wavelength for the bare TiO₂ and ZnO coated TiO₂ samples treated in an acidic H₂O₂ solution. The bare TiO₂ show a maximum value of 9.96% at a wavelength of 540 nm, while the ZnO coated TiO₂ sample shows an approximate 30% increase to 12.8% at the same wavelength (540 nm). This value is significant high using the polymer electrolyte, compared with the previously reported 3.3% IPCE using the liquid electrolyte.⁵⁰ Since the IPCE is defined as the ratio of the number of electrons in the external circuit produced by an incident photon at a given wavelength, and is uncorrected for reflective losses for optical excitation through the conducting glass electrode, the IPCE can be rationalized using the following equation.⁵¹

$$\text{IPCE}(\lambda) = \text{LHE}(\lambda) \times \varphi_{\text{inj}} \times \eta_c \quad (2)$$

where LHE(λ) is the light harvesting efficiency, φ_{inj} is the quantum yield of the electron injection from the excited dyes to the conduction band of TiO₂, and η_c is the collection efficiency of the photoinjected electrons at the back contact. The factor, LHE, related to the dye uptake in the TiO₂ surface, and is not expected to be significant in this test. For comparing the amount of adsorbed dye in both samples, the level of dye desorption in the basic 1 M NaOH solution was examined by UV–vis spectroscopy, as shown in Figure 8. Using an extinction coefficient of $\epsilon = 3748 \text{ cm}^{-1} \cdot \text{M}^{-1}$ at 535 nm (N719 dye), the number of dye molecules adsorbed on the bare TiO₂ and ZnO coated TiO₂ electrodes was found to be approximately 1.38×10^{16} and 1.32×10^{16} , respectively. Similar adsorptive dye amount demonstrates that the LHE factor cannot explain the different conversion efficiency between samples.

Because the φ_{inj} is related to the energetic discrepancy between the conduction band of TiO₂ and the excited level of the dye, the large energetic difference creates a driving force, which facilitates charge transfer from the excited dye molecules to the conduction band of TiO₂.⁵² Furthermore, the negative shift of V_{CB} by the ZnO coating can interrupt the electron tunneling of electrons excited in the lower level than the lowest unoccupied molecular orbital (LUMO) level (−3.85 eV vs E_{vac})⁵³ in the dye molecules.⁵⁴ A similar effect was discussed in the Al₂O₃ coating reported by Hagfeldt et al., who explained the negative shift in the V_{CB} in the Al₂O₃ coated sample by a blue shift in the wavelength showing a maximum intensity, even though the thick Al₂O₃ coating degraded the conversion efficiency.⁵¹ However, in this experiment, a blue shift of the IPCE spectra was not observed due to the thin ZnO coating in the cell.

The η_c is a critical factor for the enhanced conversion efficiency after the ZnO coating. Two factors should be considered; charge recombination in the electrode/electrolyte and electron transport in the nanostructured TiO₂ electrode. Since charge recombination in the electrode/electrolyte interface can cause a loss of electron collection along the nanotubular TiO₂ layer, the thin ZnO coating can retard the recombination reaction to form a thin barrier layer. Electron transport in the nanostructured TiO₂ electrode is affected by the morphology of the nanotubular structure. Compared with the commercial 3-D nanoparticles, the anodic TiO₂ nanotubes can contribute to the increase in the electron transport rate in the distribution of the reduced grain boundaries from a larger average particle size and defects. As reported previously,¹⁵ this may have a minor effect in this system. Therefore, the improvement in the IPCE can be attributed to the suppression of charge recombination by the thin ZnO coating. It was reported that a thin ZnO coating

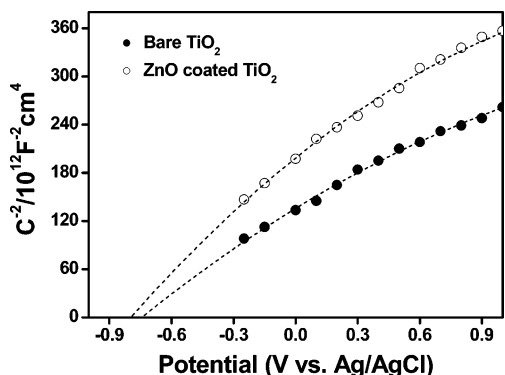


Figure 9. Mott–Schottky plots of bare TiO₂ and ZnO coated TiO₂ electrodes. The measurements were conducted at the frequency of 1 kHz with the 0.2 M LiClO₄ in acetonitrile (pH 6.2).

blocks electron flow in the back-direction (triiodides of redox electrolyte and cations of dye), which contributes to the increase in the V_{oc} of the cell. The shift toward the vacuum level of the edge potential after the ZnO coating was supported by the Mott–Schottky measurements. The behavior of charge transfer in the electrode/electrolyte interface was examined by cyclic voltammetry and open-circuit voltage decay measurements.

3.6. Mott–Schottky Plots. To confirm the negative shift of the band-edge potential, the Mott–Schottky plot of the bare and ZnO coated TiO₂ electrodes was performed at a frequency of 1 kHz at room temperature. In the Mott–Schottky analysis, a linear relationship is predicted between the applied potential and inverse square of the capacitance ($1/C^2$), arising from the space charge layer in the semiconductor.⁵⁵ Under the biasing conditions where the semiconductor space charge region is in depletion, the capacitance of the space charge region can be described as follows:

$$\frac{1}{C_{sc}} = \frac{2}{e\epsilon_0\epsilon N_d} \left(-\Delta\varphi - \frac{kT}{e} \right) \quad (3)$$

where e is electronic charge (1.6×10^{-19} C), ϵ_0 is the permittivity of free space (8.86×10^{-12} F/m), ϵ is the dielectric constant (48) of the TiO₂ material, N_d is dopant (donor or acceptor) concentration, $\Delta\varphi$ is the difference between the applied potential and the flat-band potential ($E - E_{fb}$), k is the Boltzmann constant, and T is the absolute temperature.⁵⁶ From the fact that the term of kT/e is 0.026 eV at room temperature, and was insufficient to influence the original value, the eq 4 was briefly summarized to the following:

$$\frac{1}{C_{sc}} = \frac{2}{e\epsilon_0\epsilon N_d} (E - E_{FB}) \quad (4)$$

The slope is inversely proportional to the effective donor or acceptor concentration in the semiconductor, and the flatband potential can be determined by extrapolating $C = 0$. The two assumptions were satisfied by applying the above relationships.⁵⁷ The first is that the capacitance is assumed to be the space charge capacitance. The contribution of the double layer capacitance to the total capacitance is negligible because the space charge capacitance is much smaller than the double layer capacitance (2–3 orders of magnitude). The second is that the equivalent circuit is a series combination of a resistor and a capacitance (space charge capacitance).

From Figure 9, the flatband potential of both samples was obtained. The calculated V_{FB} for the bare and ZnO coated TiO₂ electrodes were -0.735 and -0.79 V versus Ag/AgCl (in saturated KCl), respectively. The V_{FB} of nanostructure TiO₂ at

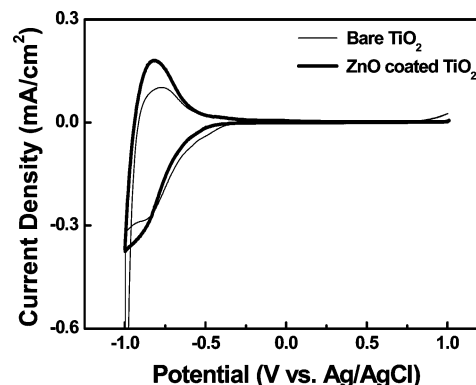


Figure 10. Cyclic voltammograms of the bare and ZnO coated TiO₂ nanotubes in the 0.1 M NaOH solution (pH 13). The scan direction with a scan rate of 50 mV/s is positive to negative potential. The active area is approximately 1 cm².

the pH 6.2 electrolyte was reported to be approximately -0.79 V versus SCE.⁵⁸ The agreeable results were obtained in this anodization system by voltage conversion between different reference electrode scales. The coating with a wide-band gap material, e.g., ZnO, built in an inherent barrier layer to block electron transfer from the conduction band or trap sites of the TiO₂ to the triiodide of the redox electrolyte. Moreover, the positive-directed slope shows that the TiO₂ materials are n-type semiconductors and a similar donor concentration from the parallel relationship of the slopes was contained in both samples. Using eq 4 and the physical constants for the TiO₂ material, the donor concentration of the bare TiO₂ and ZnO coated TiO₂ was calculated to be 1.71×10^{16} and 2.22×10^{16} cm⁻³, respectively, using a linear fitting method.

3.7. Interfacial Reaction Obtained From Cyclic Voltammetry. Figure 10 shows the cyclic voltammetry curves of the bare and ZnO coated TiO₂ electrode in the 0.1 M NaOH solution. Since cyclic voltammetry is a useful method for detecting interfacial electron flow in the TiO₂/electrolyte, the change or modification of the surface region was well caught up. Both voltammograms show hysteric shape characteristics, which suggest that electron charging/discharge occurs in the anodic TiO₂ film/electrolyte interface, indicating Faradic currents in the electrolyte. The thin ZnO coating on the TiO₂ surface induces a shift to a more negative potential region (-0.4 V vs Ag/AgCl) at the starting point of the cathodic current. This demonstrates that the ZnO coating plays a role as a blocking layer, which suppresses electron flow to the electrolyte. In addition, the ZnO coating appears to passivate the surface state or trap sites on the surface of the anodic TiO₂ nanotubes.⁵⁹ This is because the current in the positive potential of V_{FB} originates from charge transfer through the trap/surface states in the band gap of TiO₂. At this point, the Ti³⁺ states leaving the surface region participate in electron transfer. This clearly influences the electron lifetime of the photoinjected electrons in the interfacial electron transfer.

As shown in Figure 1, the electrons in the distributed trap sites were limited to react with the triiodide of the redox electrolyte due to the formation of a thin ZnO barrier layer. The result shown in Figure 6, which was measured in the dark state, demonstrates the decrease in charge recombination on the ZnO coated sample. Indeed, the magnitude and onset of the dark current indicate the extent of charge recombination between the photoinjected electrons from the excited dye molecule positioned in the LUMO, and the I₃⁻ ions in the electrolyte, assuming negligible charge recombination between the photoexcited electrons in the TiO₂ film and dye cations due to the

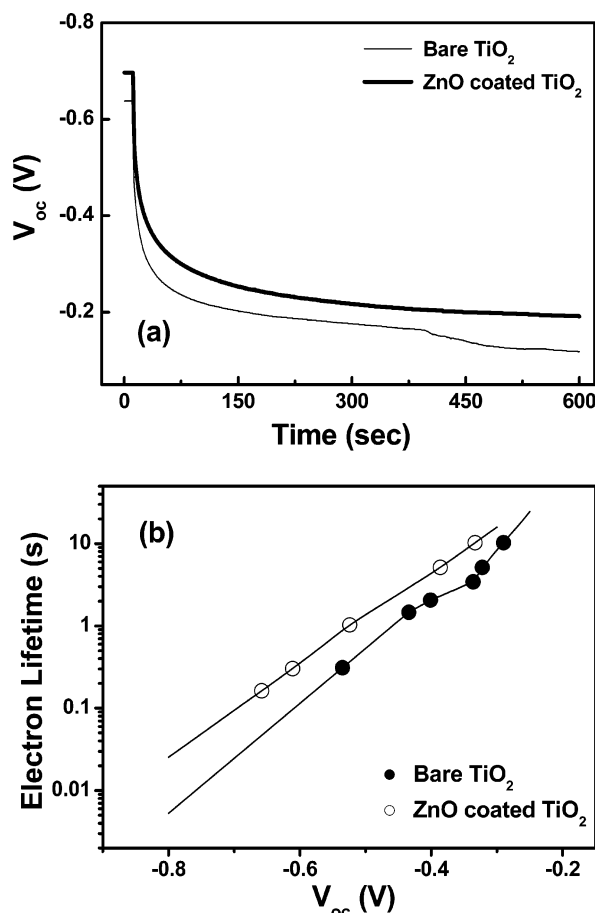


Figure 11. The curves of the open-circuit photovoltage decay (OCVD) of the bare and ZnO coated TiO_2 nanotubes. The profile of the V_{oc} decay as a function of time (a) and the log-plot of the electron lifetime as a function of V_{oc} (b).

fast kinetics in the range from μs to ns.⁶⁰ The onset of the dark current on the ZnO coated sample was shifted to a negative value, which complies with the constraint of charge recombination.

3.8. Influence of ZnO Coating. The electron lifetime was also measured using the open-circuit voltage decay (OCVD) technique. Since the electron lifetime is related to electron recombination, the OCVD technique provides information on the kinetics of charge recombination in the low photovoltage domain because the stationary illumination was abruptly disturbed. The change in the open-circuit voltage was measured as a function of time. The evolution proceeded without memory of the preceding states, which shows that the OCVD corresponds to a succession of steady states.

Figure 11a shows the exponential decay curves of V_{oc} (V) in the bare and ZnO coated TiO_2 electrodes. After 10 s illumination, exponential decay of the photovoltage occurred immediately, which was followed by a steady decrease. The ZnO coated sample showed no significant change, while the bare TiO_2 film contains an irregular curve in the low photovoltage region. From the decay curve of the photovoltage, the electron lifetime was calculated by applying eq 1. The electron lifetime as a function of V_{oc} (V) was plotted in Figure 11b. The ZnO coated TiO_2 nanotube shows a linear relationship on a logarithmic scale, which means that charge recombination is related to the first-order dependence on the electron concentration of the TiO_2 electrode. The longer electron lifetime was obtained in the scanned potential range and indicates that more electrons surviving from the back-reaction contribute to the improvement

in photocurrent. On the other hand, the linear curve of the bare TiO_2 nanotube arrays showed some deviation in the low potential region, from -0.25 to -0.35 V, indicating the formation of interfacial charge transfer from the trap/surface states to the cations of the redox electrolyte.⁶¹ Essentially, the recombination reaction in dye sensitized solar cells that occurs in a nanoporous TiO_2 film and is mediated by the electron acceptor, I_2 , is a nonlinear property that shows a second order behavior with respect to the electron concentration. This means that the effective recombination contains contributions from not only the free carriers but also the trapping, detrapping and charge-transfer mechanisms. Moreover, the minor delay in the electron lifetime through trapping and detrapping events is also expected considering the various phases TiO_2 crystallinities along the column of the nanotubes. Mostly, a charge-transfer related delay in the domain of the low photovoltage should be considered. Hence, the recovery of interfacial charge transfer was confirmed by the chemical modification in the surface region of the anodic TiO_2 nanotubes with the ZnO coating. This means that the thin ZnO coating affects the electron transfer in the anodic TiO_2 /electrolyte and enhances the electron lifetime by the blocking the back-reaction. In addition, retardation of the back-reaction becomes a factor for the improved photocurrent in the cell. This is because more electrons are collected in the conducting substrate due to a reduced loss of photoinjected electrons to the trapping sites.

Therefore, the improvement in the conversion efficiency in the anodic TiO_2 nanotube coated with the ZnO material is due to the following reasons. First, the increase in V_{oc} is caused by a negative shift in the local Fermi level by the thin ZnO coating on the anodic TiO_2 surface, which forms an inherent barrier layer that retards charge recombination in the TiO_2 /electrolyte interface. Second, the enhancement in J_{sc} may be due to electron transport of the nanotubular TiO_2 electrode resulted from the nanotubular TiO_2 assembly of the increased average crystallite size and the retardation of the unfavorable electron transfer to the back-direction (redox electrolyte) due to the barrier effect of the thin ZnO layer. If this does not occur, electron transfer is organized in the widely distributed trap sites, particularly in the low photovoltage region of -0.25 to -0.35 V. Third, the low fill factor of ZnO coated film is caused by a thickening of the TiO_2 barrier layer in the TiO_2 /Ti substrate as a result of the second-step thermal treatment, despite the blocking of the V_{oc} drop, when the redox electrolyte is closely connected to the transparent conducting substrate. The low fill factor is recovered by up to 30% through a surface treatment with acidic H_2O_2 (10 mM). From this treatment, the elimination of the remnants remaining on the nanotubular wall after the anodic reaction and the etching effect on the TiO_2 barrier layer are considered to be the major causes of the enhanced photocurrent. Therefore, the thin ZnO coating with the subsequent acidic hydrogen peroxide treatment on the anodic TiO_2 nanotubes enhance the efficiency of the solid-state dye-sensitized solar cells by approximately 30%. Under back side illumination (Pt coated side), the ZnO coating and the surface treatment with 10 mM H_2O_2 on the short nanotubular TiO_2 film under the composite polymer electrolyte shows a similar behavior in the operation of a dye cell.

4. Conclusions

Several 3 μm -thick anodic TiO_2 nanotube arrays were grown in a 0.45 wt % NaF-based electrolyte, an applied potential of 20 V, and a time of 18 h under slow magnetic agitation. This study examined the effect of a ZnO coating on the nanoporous

TiO₂ film on the conversion efficiency of a dye cell. The solid-state dye-sensitized solar cells consisted of an anodic TiO₂ film as a working electrode under backside illumination had a V_{oc} of -0.64 V, a J_{sc} of 2.38 mA/cm², a fill factor of 38%, and an efficiency of 0.578%. On the other hand, the ZnO coated TiO₂ electrode showed a V_{oc} of -0.71 V, a J_{sc} of 2.68 mA/cm², a fill factor of 37%, and an efficiency of 0.704% under back-side illumination. The almost 20% improvement from the ZnO coating was attributed to the suppressed electron flow to the back-direction, which enhanced the open-circuit voltage (V_{oc}). Moreover, the suppression of electron loss due to straight electron flow and the hindrance of charge recombination in the TiO₂/electrolyte enhanced the photocurrent, even though a polymer electrolyte with a low conductivity was used. However, the low fill factor of both samples resulted from the TiO₂ barrier layer, the application of solid-state polymer electrolyte and backside illumination, which affects the loss of charge recombination. The improvement (approximately 30%) in the fill factor was explained by the 10 mM H₂O₂ surface treatment reducing the thickness of the TiO₂ barrier layer and removing the remnant of the anodic reaction. The increased fill factor is directly related to the improvement in the conversion efficiency in the solid-state dye-sensitized solar cells. In conclusion, an approximately 1% efficiency was achieved using an anodic TiO₂ film after the surface modification by covering the thin ZnO layer in the solid-state electrolyte under back-side illumination.

Acknowledgment. This work was supported in part by KOSEF (Contract No. R01-2004-000-10143-0) and in part by the Research Center for Energy Conversion and Storage (Contract No. R11-2002-102-00000-0).

Supporting Information Available: Surface roughness according to several pH values of anodic electrolytes. This material is available free of charge via the Internet at <http://pubs.acs.org>.

References and Notes

- (1) O' Regan, B.; Grätzel, M. *Nature* **1991**, *353*, 737.
- (2) Kang, S. H.; Kim, J.-Y.; Sung, Y.-E. *J. Photochem. Photobiol., A: Chem.* **2007**, *186*, 234.
- (3) Yum, J.-Y.; Kim, S.-S.; Kim, D.-Y.; Sung, Y.-E. *J. Photochem. Photobiol., A: Chem.* **2005**, *173*, 1.
- (4) Park, K.-W.; Sung, Y.-E. *Inorg. Chem.* **2005**, *44*, 3190.
- (5) Asahi, R.; Morkawa, T.; Ohwaki, T.; Aoki, K.; Taga, Y. *Science* **2001**, *293*, 269.
- (6) Zhang, Z.; Gong, Z.; Yang, Y. *J. Phys. Chem. B* **2004**, *108*, 17546.
- (7) Lee, C. W. *J. In. Eng. Chem.* **2006**, *15*, 967.
- (8) Macak, J. M.; Tsuchiya, H.; Schmuki, P. *Angew. Chem., Int. Ed.* **2005**, *44*, 2100.
- (9) Paulose, M.; Shankar, K.; Grimes, C. A. *J. Phys. Chem. B* **2006**, *110*, 16179.
- (10) Lai, Y.; Sun, L.; Chen, Y.; Chin, J. W. *J. Electrochem. Soc.* **2006**, *153*, D123.
- (11) Grätzel, M. *J. Photochem. Photobiol., A: Chem.* **2004**, *164*, 3.
- (12) van de Lagemaat, J.; Frank, A. J. *J. Phys. Chem. B* **2001**, *105*, 11194.
- (13) Gregg, B. A. *Coord. Chem. Rev.* **2004**, *248*, 1215.
- (14) Adachi, M.; Murata, Y.; Okada, I.; Yoshikawa, S. *J. Electrochem. Soc.* **2004**, *150*, G488.
- (15) Zhu, K.; Neale, N. R.; Miedaner, A.; Frank, A. J. *Nano Lett.* **2007**, *7*, 69.
- (16) Sayama, K.; Sugihara, H.; Arakawa, H. *Chem. Mater.* **1998**, *10*, 3825.
- (17) Kay, A.; Grätzel, M. *Chem. Mater.* **2002**, *14*, 2930.
- (18) Aileron, H.; Boschloo, G.; Mendoza, P.; Hagfeldt, A. *J. Phys. Chem. B* **2005**, *109*, 18483.
- (19) Kang, S. H.; Kim, J.-Y.; Sung, Y.-E. *Electrochim. Acta* **2007**, *52*, 5242.
- (20) Bard, A. J.; Faulkner, L. R. *Electrochemical Methods*; Wiley, New York, 2001; Chapter 1.
- (21) Kim, J. H.; Kang, M.-S.; Kim, Y. J.; Kang, Y. S. *Chem. Commun.* **2004**, 1662. (Cambridge)
- (22) Kang, S. H.; Sung, Y.-E. *Electrochim. Acta* **2006**, *51*, 4433.
- (23) O'Regan, B.; Schwartz, D. T.; Zakerruddin, S. M.; Grätzel, M. *Adv. Mater.* **2000**, *12*, 1263.
- (24) Boschloo, G.; Fitzmaurice, D. *J. Phys. Chem. B* **1999**, *103*, 2228.
- (25) Bisquert, J.; Zaban, A.; Greenshtein, M.; Mora-Seró, I. *J. Am. Chem. Soc.* **2004**, *126*, 13550.
- (26) Zaban, A.; Greenshtein, M.; Bisquert, J. *J. Chem. Phys. Chem.* **2003**, *4*, 859.
- (27) Choi, J.; Wehrspohn, Ralf B.; Lee, J.; Gosele, U. *Electrochim. Acta* **2004**, *49*, 2645.
- (28) Raja, K. S.; Misra, M.; Paramguru, K. *Electrochim. Acta* **2005**, *51*, 154.
- (29) Tanaka, S.-I.; Iwatani, T.; Tanaki, T. *J. Electrochem. Soc.* **2002**, *149*, F186.
- (30) Scherrer, P. *Göttinger Nachrichten* **1918**, *2*, 98.
- (31) In *Handbook of X-Ray Photoelectron Spectroscopy*; Wagner, C. D., Riggs, W. M., Davis, L. E., Muilenger, G. E., Eds.; Perkin-Elmer: 1979.
- (32) Butler, M. A.; Ginley, D. S. *J. Electrochem. Soc.* **1978**, *125*, 228.
- (33) Wang, H.; Yip, C. T.; Xie, M. H. *Appl. Phys. Lett.* **2006**, *89*, 023508.
- (34) Diamont, Y.; Chen, S. G.; Zaban, A. *J. Phys. Chem. B* **2003**, *107*, 1977.
- (35) Roh, S.-J.; Mane, R. S.; Min, S.-K.; Han, S.-H. *Appl. Phys. Lett.* **2006**, *89*, 253512.
- (36) Mane, R. S.; Lee, W. J.; Han, S.-H. *J. Phys. Chem. B* **2005**, *109*, 24254.
- (37) Mor, G. K.; Varghese, O. K.; Grimes, C. A. *Adv. Funct. Mater.* **2005**, *12*, 1291.
- (38) Wang, Q.; Moser, J.-E.; Grätzel, M. *J. Phys. Chem. B* **2005**, *109*, 14945.
- (39) Palomares, E.; Clifford, J. N.; Durrant, J. R. *Chem. Commun.* **2002**, 1464.
- (40) Rühle, S.; Dittrich, T. *J. Phys. Chem. B* **2005**, *109*, 9522.
- (41) Cameron, P. J.; Peter, L. M. *J. Phys. Chem. B* **2003**, *107*, 14394.
- (42) Rühle, S.; Cahen, D. *J. Phys. Chem. B* **2004**, *108*, 17946.
- (43) Nogueira, A. F.; Longo, C.; De Paoli, M.-A. *Coord. Chem. Rev.* **2004**, *248*, 1455.
- (44) Jeong, Y. B.; Lee, D. Y.; Kim, S.-S.; Sung, Y.-E.; Kim, D. W. *J. Ind. Eng. Chem.* **2004**, *10*, 499.
- (45) Kang, M. Gu.; Park, N.-G.; Ryu, K. W.; Kim, K.-J. *Sol. Energy Mater. Sol. Cells* **2006**, *90*, 574.
- (46) Gregg, B. A.; Chen, S.-G.; Ferrere, S. *J. Phys. Chem. B* **2003**, *107*, 3019.
- (47) Mor, G. K.; Shankar, K.; Grimes, C. A. *Nano Lett.* **2006**, *6*, 215.
- (48) Dimitrijevic, N. M.; Saponjic, Z. V.; Rajh, T. *J. Phys. Chem. B* **2003**, *107*, 7368.
- (49) Nakade, S.; Kanzaki, T.; Kubo, W.; Yanagida, S. *J. Phys. Chem. B* **2005**, *109*, 3480.
- (50) Macak, J. M.; Tsuchiya, H.; Ghicov, A.; Schmuki, P. *Electrochem. Commun.* **2005**, *7*, 1133.
- (51) Alarcón, H.; Boschloo, G.; Mendoza, P.; Solis, J. L.; Hagfeldt, A. *J. Phys. Chem. B* **2005**, *109*, 18483.
- (52) Frank, A. J.; Kopidakis, N. van de Lagemaat, J. *Coord. Chem. Rev.* **2004**, *248*, 1165.
- (53) Lenzmann, F.; Krueger, J.; Burnside, S.; Brooks, K.; Grätzel, M.; Gal, D.; Rühle, S.; Cahen, D. *J. Phys. Chem. B* **2001**, *105*, 6347.
- (54) Yang, S.; Huang, C.; Zhai, J.; Wang, Z.; Jiang, L. *J. Mater. Chem.* **2002**, *12*, 1459.
- (55) Barsoukov, E.; Macdonald, J. R. *Impedance Spectroscopy Theory, Experiment, and Applications*; Wiley: NJ, 2005; Chapter 4.
- (56) Wang, G.; Wang, Q.; Lu, W.; Li, J. *J. Phys. Chem. B* **2006**, *110*, 22029.
- (57) Fabregat-Santiago, F.; Garcia-Belmonte, G.; Bisquert, J.; Bogdanoff, P.; Zaban, A. *J. Electrochem. Soc.* **2003**, *150*, E293.
- (58) Rothenberger, G.; Fitzmaurice, D.; Grätzel, M. *J. Phys. Chem.* **1992**, *96*, 6951.
- (59) Sayama, K.; Sugihara, H.; Arakawa, H. *Chem. Mater.* **1998**, *10*, 3825.
- (60) Palomares, E.; Clifford, John, N.; Durrant, James, R. *J. Am. Chem. Soc.* **2003**, *125*, 475.
- (61) Fabregat-Santiago, F.; García-Cañadas, J. *J. Appl. Phys.* **2004**, *96*, 6903.